Dynamics of the mixed exciton and charge-transfer states in light-harvesting complex Lhca4

Novoderezhkin, Vladimir I.; Croce, Roberta; van Grondelle, Rienk

published in
Biochimica et Biophysica Acta - Bioenergetics
2018

DOI (link to publisher)
10.1016/j.bbabio.2018.06.016

document version
Publisher's PDF, also known as Version of record

BBA - Bioenergetics 1859 (2018) 655–665

Contents lists available at ScienceDirect

BBA - Bioenergetics

journal homepage: www.elsevier.com/locate/bbabio

Dynamics of the mixed exciton and charge-transfer states in light-harvesting complex Lhca4: Hierarchical equation approach☆

Vladimir I. Novoderezhkin[a], Roberta Croce[b], Rienk van Grondelle[b,*]

[a] A. N. Belozersky Institute of Physico-Chemical Biology, Moscow State University, Leninskie Gory, 119992 Moscow, Russia
[b] Department of Biophysics, Faculty of Sciences, VU University Amsterdam, De Boelelaan 1081, 1081 HV Amsterdam, the Netherlands

ARTICLE INFO

Keywords:
Lhca4
Light-harvesting complex
Exciton states
Charge-transfer states
Redfield theory
Förster theory
Hierarchical equation of motion

ABSTRACT

We model the energy transfer dynamics in the Lhca4 peripheral antenna of photosystem I from higher plants. Equilibration between the bulk exciton levels of the antenna and the red-shifted charge-transfer (CT) states is described using the numerically inexpensive Redfield-Förster approach and exact hierarchical equation (HEOM) method. We propose a compartmentalization scheme allowing a quantitatively correct description of the dynamics with the Redfield-Förster theory, including the exciton-type relaxation within strongly coupled compartments and hopping-type migration between them. The Redfield-Förster method gives the kinetics close to the HEOM solution when treating the CT state as dynamically localized. We also demonstrate that the excited states strongly coupled with the CT should be considered as localized as well.

1. Introduction

Photosystem I (PSI) is one of the two pigment-protein complexes driving the conversion of sunlight into chemical energy in photosynthesis [1–3]. PSI from higher plants is composed of a core complex and four outer antenna subunits (Lhca1-4) assembled on one side of the core [4–6] which absorb light and transfer excitation energy to the reaction center where charge separation occurs [7–10]. Two peripheral antennae (Lhca3 and 4) are characterized by the presence of chlorophylls (Chl) *a* with absorption and emission bands around 30 nm red-shifted compared to those of the other chlorophylls associated with plant complexes [11–15]. Spectroscopic studies suggested that the red spectral forms originate from a mixing between the excited and charge transfer (CT) states within tightly packed Chl dimers [16–20]. It was shown that the CT state can be abolished when the ligand for one of the two Chls in the dimer (Chl 609, following the nomenclature of Liu et al. [21]), which is an Asn in Lhca4-WT, is substituted by an His [17,19]. This mutant is called NH in the following. Quantitative modeling of the absorption, linear dichroism, fluorescence and Stark spectra of the wild-type (WT) Lhca4 and the NH mutant enabled to build an exciton model of Lhca4, determine the origin of the CT state, and define its parameters and the degree of mixing with the excited states [22]. This model is based on the modified Redfield (mR) approach [23], giving a realistic lineshape of the exciton (and mixed exciton-CT) components due to including of strong exciton-phonon coupling.

In principle, the mR picture makes it possible to explore the excitation dynamics of the complex (using the parameters extracted from the fit of the available steady-state spectra). A more realistic description can be obtained using the recently developed generalization of the mR, i.e. the coherent modified Redfield (cmR) theory [24–26], containing transfers between the one-exciton populations (similarly to the mR theory) together with the decay of the one-exciton coherences (not included in the mR). However, the cmR does not include the non-secular transfers between populations and coherences. It was demonstrated that due to this shortcoming the cmR gives unrealistically fast transfers between weakly coupled and isoenergetic sites [27]. In such a weakly coupled configuration the coherence (between almost isoenergetic exciton eigenstates) is slowly oscillating and long-lived, being continuously re-pumped via quasi-secular transfers from the populations. In the site representation the existence of such coherence will keep excitations localized at the initially excited site for a long time, whereas in the secular approximation (with fast decay of the coherences) the excitation will be quickly delocalized between the donor and acceptor sites, looking like unexpectedly fast transfer [27,28]. The simplest way to exclude this artifact is to split the whole system into several compartments containing strongly coupled pigments with big exciton splitting. The dynamics within such clusters can be described by mR/cmR, whereas transfers between the weakly coupled clusters can be

☆ This article is part of a Special Issue entitled 20th European Bioenergetics Conference, edited by László Zimányi and László Tretter.

* Corresponding author.
E-mail address: r.van.grondelle@vu.nl (R. van Grondelle).

https://doi.org/10.1016/j.bbabio.2018.06.016
Received 21 March 2018; Received in revised form 5 June 2018; Accepted 29 June 2018
Available online 05 July 2018
0005-2728/

modeled using the generalized Förster theory [29]. This combined Redfield-Förster approach can be justified by comparing it with exact methods, for example the hierarchical equation of motion (HEOM) [30,31].

In recent studies a comparison of the HEOM and Redfield-Förster models with different compartmentalization schemes has been done for the major plant light-harvesting from higher plants LHCII [27,32]. In this paper we perform a similar analysis for Lhca4 complex, containing the CT state. Notice that the modeling with including the exciton-CT mixing is more challenging than modeling of just exciton dynamics. The CT state is more strongly coupled to the environmental degrees of freedom, including fast nuclear motion. As a result, the CT is characterized by a larger displacement of its potential energy surface along effective nuclear coordinates (as compared to the usual excited states). Therefore, the exciton-CT mixing is not uniform, being more pronounced near the crossing point, whereas near the bottom of the CT potential the excitation is localized. This situation is far beyond the limits of the Redfield theory (where the transfers are treated as exciton-type relaxation between delocalized states). One can expect that the problem can be solved by applying the generalized Förster theory for modeling the transfers between the exciton and localized CT states. But the task is not trivial, because the exciton-CT mixing generally makes the involved exciton states localized as well, thus changing their mixing with other exciton states of the complex (as we will see below). The main goal of this work is to develop the cmRgF approach (with a suitable compartmentalization of the whole complex) allowing a quantitatively correct description of the dynamics, i.e. yielding kinetics that are not significantly different from those obtained with the exact HEOM solution.

In Section 2 we describe the model of Lhca4 with a simplified (single-component) spectral density that is convenient to use in the calculation of the population dynamics with the HEOM. In Section 3 we perform a comparative study of the cmRgF and HEOM kinetics (doing it consequently for different parts of the complex). This allows a deeper understanding of the specifics of the exciton → CT transfers, and also leads us to the optimal compartmentalization scheme for the whole antenna. This compartmentalization (verified by the exact HEOM method) opens the gate to using the advantages of the cmRgF approach allowing a numerically inexpensive calculation of various linear and nonlinear spectral responses with arbitrary spectral density (including a multi-component one approximating the experimentally measured spectral density). Averaging over disorder and improving the fit using an evolutionary-based search also became available. Note that evaluation of the 3rd-order nonlinear responses (transient absorption, photon echoes, etc.) with exact methods is too expensive numerically (note that in practice the HEOM modeling is most often restricted to the 2nd-order population dynamics for a single realization of the disorder).

2. The model

The pigment arrangement in Lhca4 [5] is shown in Fig. 1. Following our recent study [22] we use the 13-state model of reconstituted Lhca4, containing 9 chlorophylls (Chls) *a* (602–604, 609–614), 3 Chls *b* (606–608) and one charge-transfer (CT) state corresponding to a charge separation between *a*603 and *a*609. The site energies, exciton couplings and disorder values for the 13 diabatic states are the same as in [22], where they have been extracted from the fit of optical spectra for the wild-type (WT) and NH mutant (lacking the CT state). In the original model [22] we used the experimental spectral density including a coupling to low-frequency phonons (parametrized in the form of an overdamped Brownian oscillator) and coupling to a manifold of high-frequency vibrations. In the present study we use a simplified spectral density in the form of a single overdamped Brownian oscillator. The characteristic frequency (damping constant) is taken to be large enough ($\gamma = 500\,cm^{-1}$) to guarantee realistic rates for both intra- and inter-band (Chls *b* → Chls *a*) transfers. Such a model is capable to reproduce the spectral profiles (see Fig. 1), although some features in absorption (OD) and fluorescence (FL) determined by coupling to high-frequency modes (1200–1500 cm^{-1}) are missing (see for example, the shoulder around 740 nm in the FL spectrum for the NH mutant).

The model with the simple spectral density allows a nonperturbative calculation of the excitation dynamics (with routinely available computational facilities) using the hierarchical equation of motion (HEOM). The exact HEOM solution can be then compared with other (perturbative) approaches, like standard Redfield theory (sR), coherent modified Redfield (cmR), coherent modified Redfield combined with the generalized Förster theory (cmRgF), as we did in our recent study of the dynamics in LHCII (see [27]) containing the description of the corresponding equations of motion. Notice that in the case of LHCII the scaled HEOM [31] with a single-component spectral density gives converging results already at small cutoff values of N_c = 3–4, where N_c is the depth of the hierarchy given by the sum of the integers describing the state of the phonon bath [27]. But in the presence of CT states (that are more strongly coupled to phonons) the depth of the hierarchy should be increased in order to describe correctly the influence of phonons on the kinetics. We have found that in the case of the Lhca4 complex (where the phonon coupling for CT is 3.2 times larger than for usual excited states [22]) the cutoff value should be increased to N_c = 6–8.

In all numerical examples (presented in the next section) the kinetics have been calculated at room temperature with the same parameters as in Fig. 1. We use the scaled HEOM [31] with the number of temperature correction terms K = 0 or 1. In the non-secular Redfield calculations we did not find any violation of the positivity of the density matrix (similarly to our studies of LHCII [27]). Notice that in the fit shown in Fig. 1 we calculate the spectra averaged over disorder. But in the numerical examples of the kinetics the calculation is performed for a single realization of the disorder corresponding to unperturbed values of the site energies.

3. Results

3.1. Equilibration between the excited a603 and CT state (N = 2 model)

As a first example we consider the transfers between the *a*603 and CT states (neglecting their coupling to the remaining states of the complex). According to our current model [22] *a*603 is the red-most pigment of the complex strongly coupled to the CT state (that is even more red-shifted). Generally the CT state is more strongly coupled to phonons than the excited *a*603 state. We then suppose that the *a*603 and CT states are described by an electron-phonon spectral density with the same characteristic frequency ($\gamma = 500\,cm^{-1}$), but with different couplings λ_{ex} and λ_{CT} (that are equal to the reorganization energies of the *a*603 and CT states, respectively). To understand how the ratio of couplings $V_{CT} = \lambda_{CT}/\lambda_{ex}$ affects the dynamics we explore three models with V_{CT} = 1, 1.5, and 3.2 (keeping the λ_{ex} value fixed at 350 cm^{-1}). The results are shown in Fig. 2.

In Fig. 2 we illustrate a configuration of the potential surfaces using a simplified one-dimensional picture. In fact each site is coupled to a manifold of nuclear modes (corresponding to different coordinates). The version of HEOM used in our modeling implies that nuclear modes acting on different sites are uncorrelated, i.e. each site has its own bath [30,31]. The manifold of the modes coupled to any site modulate its energy. For example, a reorganization of some nuclear mode will change the energy of the corresponding site, thus changing the character of its mixing with other sites. In this way, the mixing of the sites depends on the state of their baths. In the model of overdamped Brownian oscillator the state of the bath is described by some number reflecting the combined action of a continuum of modes without considering explicitly their coordinates [30,31].

In the case of N = 2 sites such a model allows a description of dynamic localization if the two states have different couplings to phonons

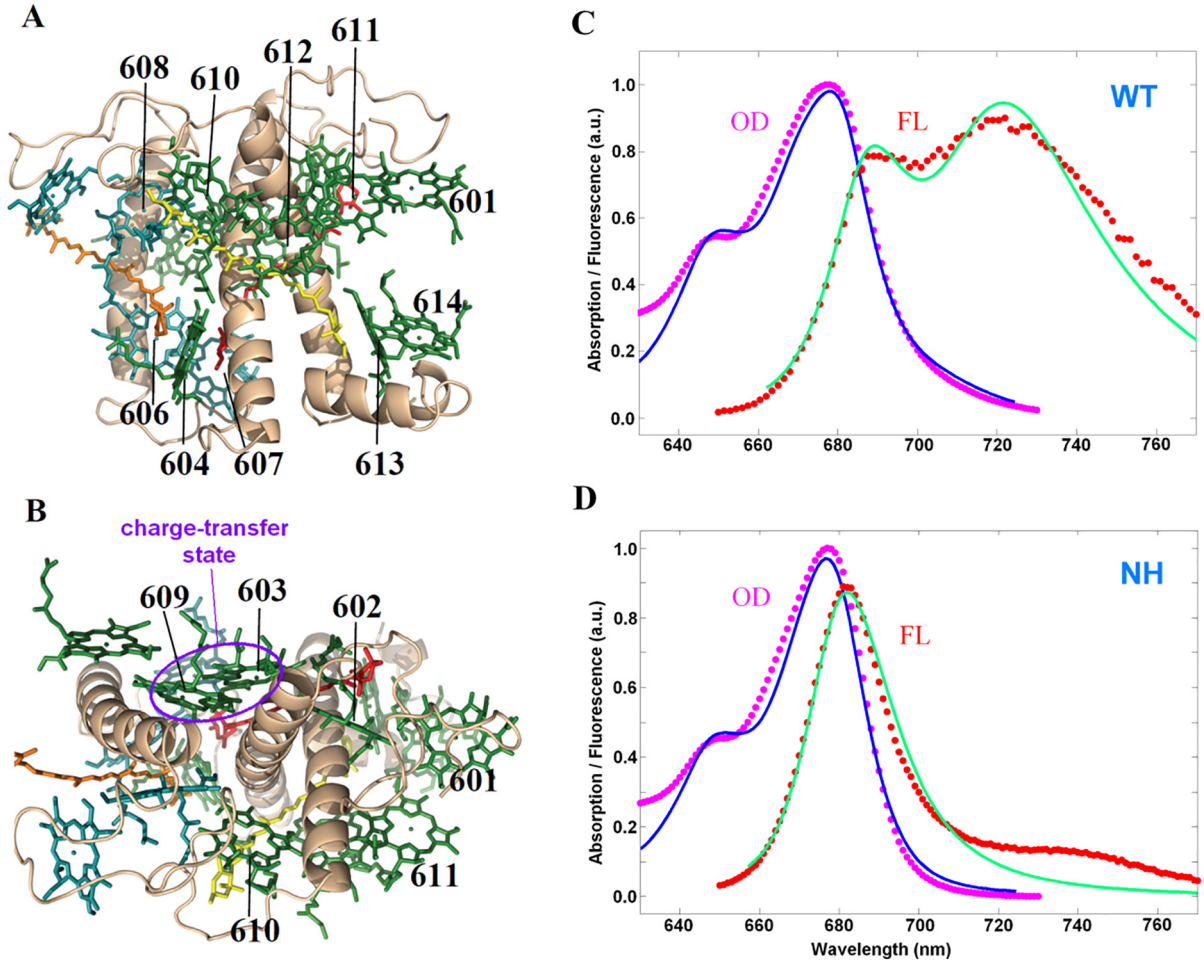

Fig. 1. Structure and optical spectra of the Lhca4 complex. (**A**,**B**) Arrangement of light-harvesting pigments in Lhca4 [5] with a view perpendicular to the membrane normal (**A**) and along the membrane normal from the stromal side (**B**), including Chls *a* (green), Chls *b* (blue), lutein (yellow), violaxanthin (red), and β-carotene (orange). The two pigments involved in the charge-transfer state (i.e. *a*603 and *a*609) are encircled by violet. (**C**,**D**) Modeling of the room temperature absorption (OD) and fluorescence (FL) spectra for the WT (**C**) and NH mutant (**D**) of Lhca4. The measured OD and FL profiles are shown by magenta and red points, respectively. Calculation (blue and green lines) is done with the mR theory using a spectral density in the form of a single overdamped Brownian oscillator with the characteristic frequency (damping constant) $\gamma = 500\,cm^{-1}$ and coupling (reorganization energy) of $\lambda = 350$ and $1120\,cm^{-1}$ for the excited and CT states, respectively. Other parameters are the same as in our 77 K Lhca4 model [22], but with some site energies adjusted, i.e. a604, b606, 607, and 608 are shifted by −40, 15, −75, and $45\,cm^{-1}$, respectively compared to the E2 set from [22]. In addition all the site energies have been uniformly red-shifted by $160\,cm^{-1}$ (to compensate for the reduced reorganization shift when switching from a realistic to the simplified single-component spectral density).

(as in the pair of *a*603 and CT states). A larger reorganization shift of one site (CT) will break its mixing with the other site (excited *a*603 state) and will localize the excitation near the bottom of the CT potential. But if we suppose that the two sites have equal phonon couplings, they will exhibit equal reorganization shifts, and therefore, their mixing (and delocalization degree) will not depend on the reorganization dynamics. In this respect the HEOM picture with overdamped Brownian oscillator resembles the one-dimensional model, where each mode is characterized by a single coordinate for all the sites (for more detailed discussion of these features see Section 4.4). This one-dimensional picture (used in Fig. 2) is convenient as a rough visualization, but one should bear in mind that in fact the model is dealing with uncorrelated phonon-induced modulations of the site energies, determined by many coordinates (although they are not included explicitly).

Notice also that in the Redfield picture the coupling of the electronic states is independent on nuclear coordinates. This situation can be illustrated by the two equally displaced potentials (even if they have different phonon couplings!) giving always uniform mixing.

The case $V_{CT} = 1$ can be illustrated (see Fig. 2) by the two potential surfaces of the diabatic states (*a*603 and CT) that have equal displacements and their mixing is uniform both in the HEOM and in Redfield picture (cmR and sR). At $V_{CT} > 1$ the displacements of the diabatic states are not equal in the HEOM picture (as shown in the right column in Fig. 2), and one can expect that the mixing of the two potentials is more pronounced near the crossing point, whereas near the bottom of the CT potential the excitation is almost localized (with some negligible admixture of *a*603). But in the Redfield picture the mixing is still considered as uniform even at $V_{CT} > 1$. Thus, one can expect deviation of the Redfield kinetics from the exact HEOM solution at $V_{CT} > 1$.

The Redfield kinetics calculated for various V_{CT} values are shown in the 1st (cmR) and 2nd (sR) columns in Fig. 2. Populations of the diabatic *a*603 and CT states at equilibrium are not strongly dependent on V_{CT}. This is expected because contributions of *a*603 and CT to the lowest state (predominantly populated at equilibrium) are not dependent on V_{CT} in the case of uniform mixing. Notice, however, that larger V_{CT} values produce an increasingly larger reorganization red shift of the lower state (due to the predominant contribution of CT to this state). Due to this shift the lower state becomes more populated at thermal equilibrium, and correspondingly, the steady-state population of the CT state is increased as well (as shown in Fig. 2).

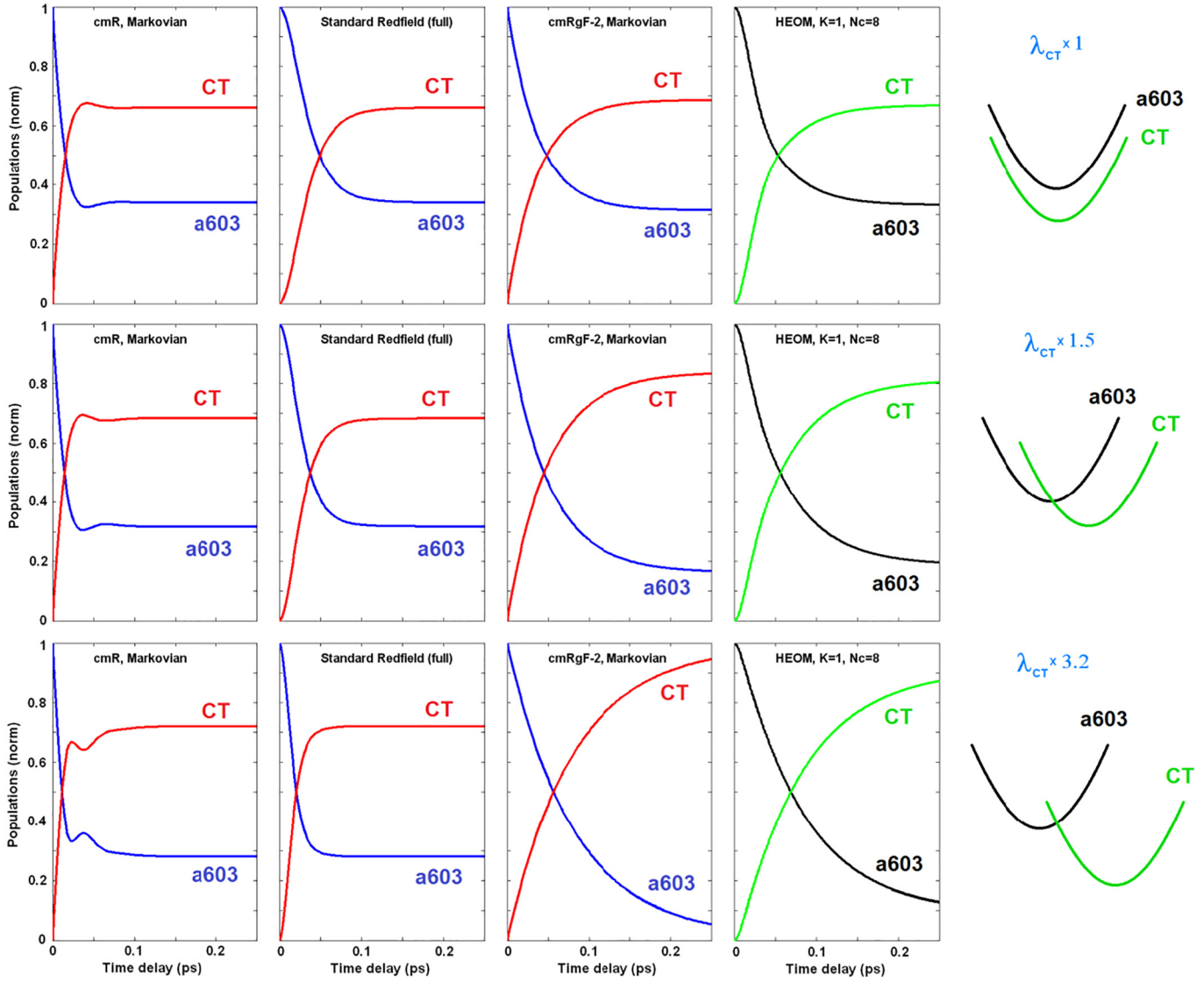

Fig. 2. Energy transfer between the *a*603 and CT states (N = 2 model). Population kinetics in the site (diabatic) representation (up to 0.25 ps delay) are calculated upon initial excitation of *a*603 for a single realization of the disorder (with unperturbed energies of the diabatic *a*603 and CT states). The calculation is done with four different theories, i.e. with cmR, sR (with the full relaxation tensor), and cmRgF-2 (identical to the pure Förster description at N = 2), as well as with the exact HEOM method. The relaxation tensors in cmR, cmRgF-2, and sR are calculated in the time-independent Markovian limit (meaning with infinitely fast bath relaxation). The ratio of electron-phonon couplings for the CT and excited states $V_{CT} = \lambda_{CT}/\lambda_{ex}$ is 1 (top), 1.5 (middle), and 3.2 (bottom) (with $\lambda_{ex} = 350\ cm^{-1}$). The corresponding displacements of the diabatic *a*603 and CT potentials in a simplified one-dimensional picture are shown schematically on the right (for the HEOM case only). Remind that in the Redfield picture the mixing of the potentials is always uniform (corresponding to equally displaced states). In the Förster limit we can formally consider the same configuration as for HEOM, but one should bear in mind that in this case the mixing of these potentials is neglected. (For interpretation of the references to color in this figure, the reader is referred to the web version of this article.)

The rates of *a*603 → CT transfer in the Redfield picture (1st and 2nd columns in Fig. 2) increase in proportion to V_{CT} at fixed λ_{ex} (because the Redfield rates are proportional to the phonon couplings). Notice that in cmR the transfers are faster due to the quick decay of the coherences between eigenstates, whereas in sR these coherences are more long-lived due to non-secular terms.

In the cmRgF-2 model we break the system into 2 weakly coupled compartments. In the case of the *a*603-CT dimer each compartment contains just a single state, i.e. the *a*603 or the CT state. It means that cmRgF-2 in this case is identical to pure Förster (describing transfer between two localized and non-mixed states). Notice that in the Förster picture the displaced configuration of the potentials is included explicitly when calculating the overlap integral, but the mixing of the potentials is neglected. The corresponding kinetics are shown in the 3rd column in Fig. 2. In the Förster model the lower state is always localized at CT (without any admixture of *a*603), and its population increases with V_{CT} due to reorganization effects increasing the energy gap between the localized *a*603 and CT states. In contrast to the Redfield picture, the transfer rate is almost independent of V_{CT} being proportional to the square of the electronic coupling between the two states according to the Förster formula (some dependence on V_{CT} still exists because V_{CT} affects the overlap of the phonon wavefunctions of the donor and acceptor due to changes in homogeneous broadening and reorganization shift).

In the HEOM picture the two displaced potentials are mixed and this mixing is dependent on the nuclear coordinate. This is in contrast to the Förster picture, where there is no mixing between the states. As a result, the HEOM kinetics reveal more delocalization (the difference in the steady-state populations of *a*603 and CT is slightly less than in the localized Förster limit (compare 4th and 3rd columns in Fig. 2).

Comparing all four columns in Fig. 2 we conclude that for the transfers to the dynamically localized CT state the exact solution (HEOM) is much closer to the Förster limit than to the Redfield picture. In the Redfield picture the displacements of the diabatic states with respect to each other is ignored, so that the mixing between them is always uniform. This picture can be used as a rough approximation to a manifold of purely excited states if they are relatively weakly coupled to phonons. But such a model is not realistic in the presence of CT that is characterized by an enhanced phonon coupling producing a large displacement with respect to the excited states.

3.2. Equilibration within the a602-603-609-CT cluster (N = 4 model)

Now we switch to the dynamics within the strongly coupled cluster of four diabatic states a602-603-609-CT. The a602 and 609 states are higher in energy than a603, but the a609 state is very strongly coupled to a603, so that the lowest eigenstate of the complex (containing a superposition of CT and a603) also has a sizable admixture of a609 (for more details see [22]).

The Redfield approach (with equal displacements and uniform mixing of the 4 states) predicts very fast equilibration (see the cmR and sR kinetics in Fig. 3). In the steady-state limit (reached within 100 fs) there is significant population of a603 and a609 that are strongly mixed with the CT state and, therefore, contribute to the lowest eigenstate (where their joint contribution is comparable with the contribution from CT). This is in contrast to the exact HEOM dynamics, where the CT is mixed with the excited states only near the crossing point. At large delays (with respect to the phonon reorganization time scale) the CT state that is dynamically localized, i.e. the excitation is equilibrated near the bottom of the CT potential, where CT contains no significant admixture of a603 and a609. The whole dynamics in the HEOM approach is slower than in the Redfield picture, where equilibration is determined by fast exciton relaxation (compare the cmR/sR and HEOM kinetics in Fig. 3). In the steady-state limit HEOM predicts predominant population of the dynamically localized CT state, again in contrast to delocalized Redfield model.

Now we will try to find some compartmentalization scheme allowing to reproduce the exact HEOM kinetics using the combined Redfield-Förster approach.

At first glance (according to the previous N = 2 example) the Redfield picture can be corrected by breaking the coherences between the CT and the other states. For example one can split the N = 4 cluster into 2 compartments, containing pure exciton states a602-603-609 and CT, respectively (cmRgF-2 model). But such a scheme gives too fast a609 → a603 transfer upon initial excitation of a609 (compare HEOM and cmRgF-2 frames in Fig. 3). The same dynamics is observed with splitting into three compartments, i.e. a602, a603–a609, and CT (cmRgF-3a model). Breaking the a603–a609 mixing results in a more correct a609 decay, as obtained with the models with 3 or 4 compartments, i.e. cmRgF-3b (a602–a609, a603, and CT), cmRgF-3c (a602–a603, a609, and CT), and the cmRgF-4 model (a602, a603, a609, and CT), corresponding to the pure Förster limit. Notice, however, that the cmRgF-3b model gives too fast equilibration between the isoenergetic and weakly coupled a602–609 sites (see black curve showing fast rise of the a602 population, that is absent in the cmRgF-3c and cmRgF-4 models as well as in the HEOM solution).

Thus, we have found two suitable models, i.e. cmRgF-3c and cmRgF-4, giving almost the same kinetics as HEOM. The most intriguing question is why we need to break the coherence between the strongly coupled a603–609 pair in these models? We have seen in Section 3.1 that the coherence between the two strongly coupled states (a603 and CT, N = 2 model) should be broken if these states have different displacements along nuclear coordinates. Large displacement with respect to each other makes these states dynamically localized even if they are strongly coupled, meaning that the exciton mechanism does not give an adequate description of the relaxation process. The

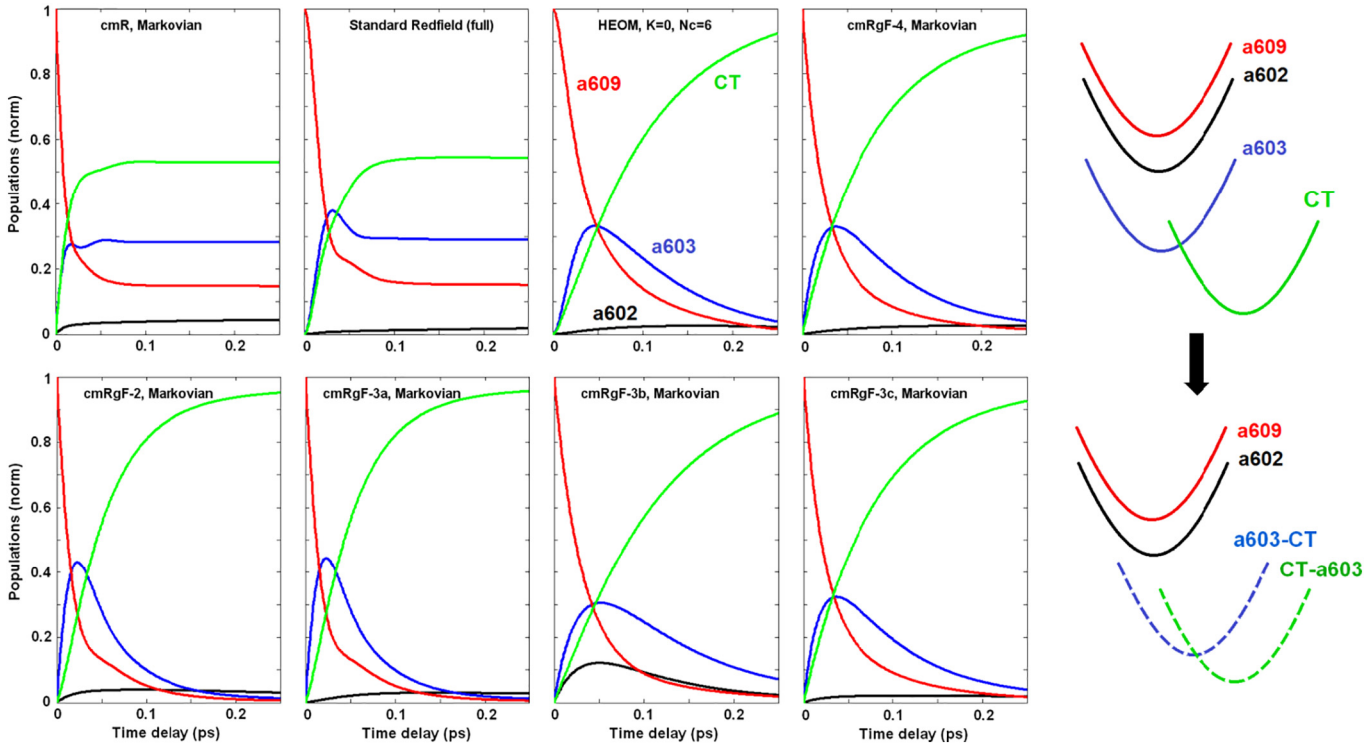

Fig. 3. Dynamics within the a602-603-609-CT cluster (N = 4 model) at V_{CT} = 3.2 upon a609 excitation for a single realization of the disorder (with unperturbed site energies). Kinetics (on the timescale of 0.25 ps) are calculated with the cmR, sR, HEOM, and Redfield-Förster models with different compartmentalization schemes, i.e. cmRgF-2 (a602-a603-a609 and CT), cmRgF-3a (a602, a603–a609, and CT), cmRgF-3b (a602–a609, a603, and CT), cmRgF-3c (a602–a603, a609, and CT), and cmRgF-4 (a602, a603, a609, and CT). Configurations of potential surfaces on the right show schematically the diabatic a602-a603-a609-CT states (top scheme) and the same potentials after mixing of the a603 and CT states (bottom scheme).

mixing of the states in the N = 4 model is more complicated. Let us consider it in two steps. We start with the configuration of the 4 diabatic states, where the CT is displaced with respect to the three excited states *a*602-603-609 (top right scheme in Fig. 3). First lets mix the CT and *a*603 state. It is reasonable to suppose that the mixing of localized CT and *a*603 induces some additional displacement of the *a*603 (with respect to *a*602 and 609), thus making it dynamically localized too. Secondly, we have to calculate the superposition of the two mixed levels (*a*603-CT and CT-*a*603) with *a*602 and 609 (bottom right scheme in Fig. 3). Obviously, the displacement of the *a*603-CT level will break its exciton-type mixing with *a*602 and 609.

We conclude that the mixing of the localized CT state with the exciton states (within some strongly coupled cluster) will make these exciton states localized. Thus, in our N = 4 example we have to treat each of the 4 states (*a*602, *a*603, *a*609, and CT) as localized and calculate the transfers between them by Förster theory. Notice, however, that in our particular case mixing of *a*603 with *a*602 can be formally included (leading us to the cmRgF-3c model) because these sites are not so strongly coupled (33 cm^{-1}) and separated by a big energy gap (166 cm^{-1}), meaning that they are localized even within the exciton picture. That is why there is no sizable difference between the cmRgF-3c and cmRgF-4 kinetics in Fig. 3.

3.3. Equilibration within the stromal- side layer (N = 8 model)

In Fig. 4 we explore the equilibration within the whole stromal-side layer, containing N = 8 states, including the *a*602-*a*603-*a*609-CT cluster (studied in the previous section), the *a*610-*a*611-*a*612 trimer and one Chl *b* site, i.e. *b*608. The Redfield picture (see the cmR and sR frames in Fig. 4) overestimates the population of *a*603 and *a*609 due to strong exciton-type mixing of these states with CT (as expected from the analysis of the separate *a*602-*a*603-*a*609-CT cluster in Section 3.2). To obtain a realistic dynamics we have to break the *a*602-*a*603-*a*609-CT cluster into 3 compartments, i.e. *a*602–*a*603, *a*609, and CT. Including the *a*610-*a*611-*a*612 trimer as the 4th and the monomeric *b*608 as the 5th compartments, we obtain the Redfield-Förster cmRgF-5 model. This model gives too fast equilibration within the *a*610-*a*611-*a*612 trimer (Fig. 4). To correct it we split the trimer into *a*610 and *a*611–*a*612 compartments, obtaining the cmRgF-6 model, that gives the kinetics that are very close to the exact HEOM solution (compare the two right frames in Fig. 4).

Notice that in our model of Lhca4 [22] *a*610 is shifted to the blue from *a*611–*a*612 (in contrast to LHCII, where these three sites are almost isoenergetic [27,34]). Being strongly (50 cm^{-1}) coupled to the blue-most *b*608 and not so strongly (25 cm^{-1}) coupled to *a*611–612, the *a*610 state is quickly populated from *b*608, with subsequent slower *a*610 → *a*611-*a*612 transfer (as shown by HEOM kinetics). Treating the *a*610-*a*611-*a*612 trimer as one excitonically coupled cluster gives unrealistically fast population of *a*611–*a*612 (compare the cmRgF-5 and cmRgF-6 schemes).

It is interesting that the standard Redfield gives more realistic dynamics within the *a*610-*a*611-*a*612 trimer as compared with the cmR and cmRgF-5 approaches, where the transfers within the coupled *a*610-*a*611-*a*612 sites are described in the secular approximation. Fast decay of the coherences results in quick delocalization with population of all the three sites. In sR with the full relaxation tensor the localization at *a*610 (after its population from *b*608) exists for a longer time due to long-lived dynamic coherence (i.e. coherence between the exciton eigenstates) maintained via non-secular transfers from populations.

Another feature appearing in the sR model is the very slow dynamics of the *b*608 depopulation. The reasons for this issue will be discussed in Section 3.5.

3.4. Equilibration within the lumenal-side layer (N = 5 model)

Fig. 5 shows the dynamics within the lumenal-side layer, containing N = 5 states, i.e. two Chl's *b* (*b*606–*b*607), intermediate blue-shifted Chl *a* (*a*604), and the Chl *a* dimer (*a*613–614). The HEOM kinetics can be satisfactory reproduced by the Redfield-Förster model with three compartments, i.e. cmRgF-3 (*a*604–*b*606, *b*607, *a*613–*a*614). Such compartmentalization is the same as we used for LHCII [27], but we break the coherence between the *b*606–*b*607 sites (because in our model of Lhca4 these states are closer in energy than in the LHCII model).

The transfers from Chl's *b* and bottleneck *a*604 state to the *a*613–*a*614 dimer are expected to be very slow (similar transfers in LHCII occur with a time constant of about 30 ps [34]). On the 1.25 ps timescale used in Fig. 5 the *a*613–*a*614 populations are negligible.

3.5. Equilibration within the whole Lhca 4 complex (N = 13 model)

Combining the cmRgF-6 (N = 8) and cmRgF-3 (N = 5) models for the stromal- and lumenal-side layers we obtain the cmRgF-9 (N = 13) model of the whole Lhca4 complex. This model yields the energy transfer kinetics that are close to the exact HEOM solution, as shown in Fig. 6. On the other hand, the pure Redfield models are not suitable, giving some artifacts. Thus, the cmR model predicts too fast equilibration within the *a*610-*a*611-*a*612 trimer, too big population of the *a*603–*a*609 sites, and unrealistically fast decay of the bottleneck *a*604 site (due to overestimated delocalization between the *a*604 and stromal side Chl's *a*). The sR model gives more realistic dynamics within *a*610-*a*611-*a*612, correct kinetics of *a*604 population, but the *a*603–*a*609 populations still remain overestimated.

Another limitation of the sR approach is connected with the one-

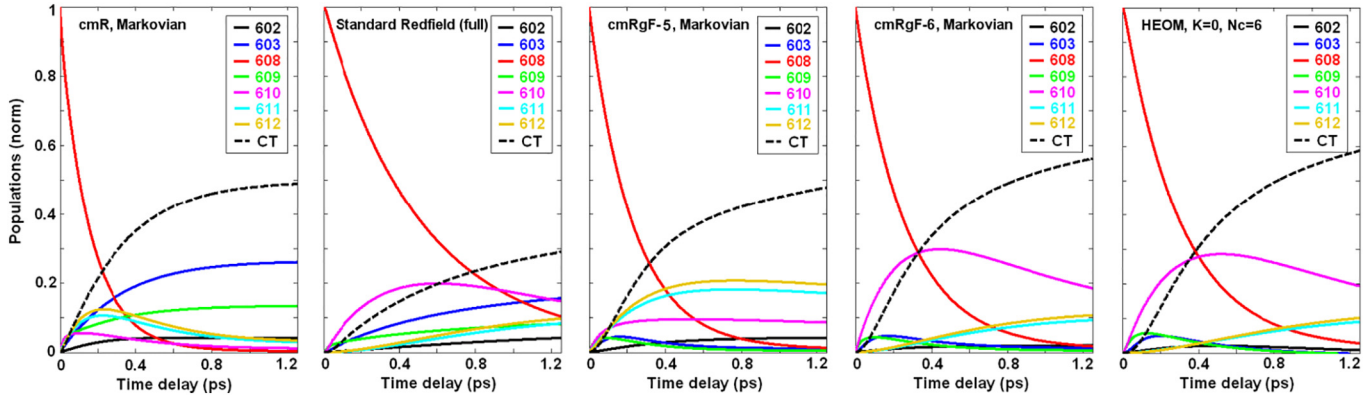

Fig. 4. Dynamics within the stromal-side pigments *a*602-*a*603-*b*608-*a*609-*a*610-*a*611-*a*612-CT (N = 8 model) upon excitation of the *b*608 site (with unperturbed site energies and V_{CT} = 3.2). Kinetics (on the timescale of 1.25 ps) are calculated with the cmR, sR, HEOM, and Redfield-Förster models with different compartmentalization schemes, i.e. cmRgF-5 (*a*602–*a*603, *a*609, CT, *a*610-*a*611-*a*612, *b*608), cmRgF-6 (*a*602–*a*603, *a*609, CT, *a*610, *a*611–*a*612, *b*608).

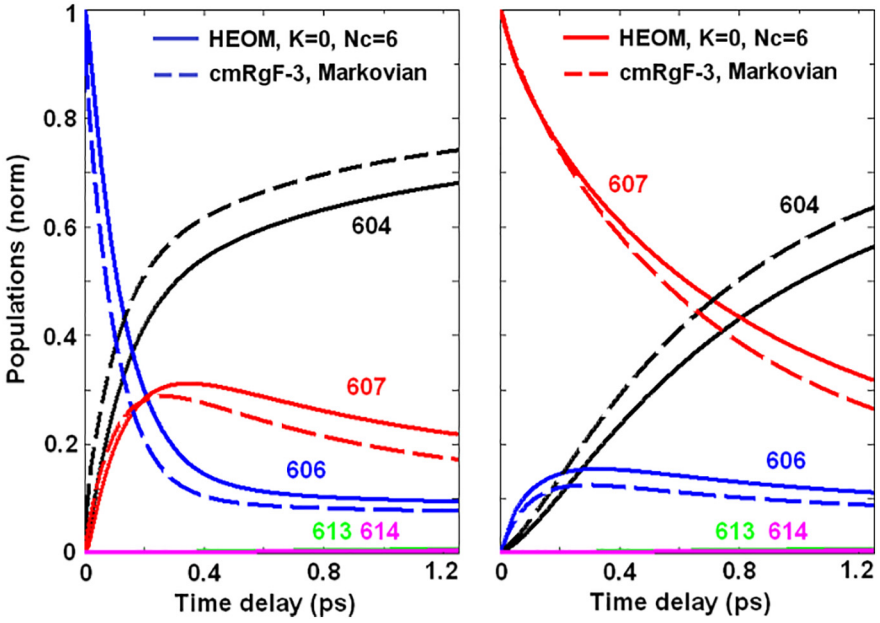

Fig. 5. Dynamics within lumenal-side pigments *a*604-*b*606-*b*607-*a*613-*a*614 (N = 5 model) upon excitation of the *b*606 (left) or *b*607 (right) with unperturbed site energies and V_{CT} = 3.2. Kinetics (on the timescale of 1.25 ps) are calculated with the HEOM, and Redfield-Förster model cmRgF-3 (*a*604–*b*606, *b*607, *a*613–*a*614). (For interpretation of the references to color in this figure, the reader is referred to the web version of this article.)

phonon character of the relaxation (arising from the weak exciton-phonon coupling approximation). As a result the transfers between the states separated by big energy gaps are too slow. Thus, the $b \rightarrow a$ transfers on the stromal side (with the fastest *b*608 → *a*609, *a*610 channels) are noticeably slower than in HEOM. On the other hand, the $b \rightarrow a$ transfers on the luminal side (i.e. *b*606 → *a*604 and *b*607 → *a*604 transfers corresponding to smaller gaps) are satisfactory reproduced, i.e. they are almost the same as in HEOM (compare the sR and HEOM frames in Fig. 6).

Quantitative comparison of the kinetics obtained with HEOM and cmRgF-9 model is shown in Fig. 7. Note some differences in the *b*607 kinetics at small delays (< 0.2 ps) connected with a break of the *b*606–*b*607 coherences in the cmRgF-9 model.

3.6. Spectral lineshapes

Now we wish to compare the spectral lineshapes emerging from the theoretical approaches that have been tested in the previous sections. We have seen that different approaches give different transfer rates between the eigenstates of the complex. In addition, the properties of eigenstates (transition dipoles (determined by delocalization), transition energies (including exciton-, reorganization- and disorder-induced shifts), and phonon-induced homogeneous broadening) are also different within the approaches used in our modeling. To illustrate this we explore the absorption (OD) spectrum of Lhca4 for a single realization of the disorder, i.e. the same as used for modeling of the kinetics in Fig. 6. We calculate the OD profile using (i) the modified Redfield (mR), (ii) combined mRgF-9 approach, (iii) complex time-dependent Redfield (ctR) theory [35], and (iv) HEOM. Notice that mR and mRgF-9 correspond to the steady-state limit of the Markovian versions of cmR and cmRgF-9 theories, respectively. The results are shown in Fig. 8.

We remind that in modified Redfield the absorption spectrum is calculated by explicitly including the diagonal exciton-phonon coupling [23], whereas off-diagonal coupling is given by a phenomenological Markovian term responsible for a relaxation-induced broadening and determined by the inverse lifetime of the exciton states [28,36]. The ctR model is based on non-phenomenological and non-Markovian treatment of the off-diagonal coupling [35]. Typically, ctR predicts significant non-uniform red-shifting of the exciton transitions (as compared to mR) [27]. This can be compensated by renormalization of the site energies in the mR approach. In Fig. 8 we uniformly shift the mR and mRgF spectra to make their comparison with the ctR theory easier.

Both mR and ctR give an intense red shoulder due to mixing of the exciton and CT states. Notice that such a mixing is calculated in the mR and ctR theories in a pure exciton basis, i.e. the mixing of the diabatic states is supposed to be uniform (corresponding to equally displaced potentials). Such exciton-type mixing produces delocalized states, including the lowest state with predominant contribution of the forbidden

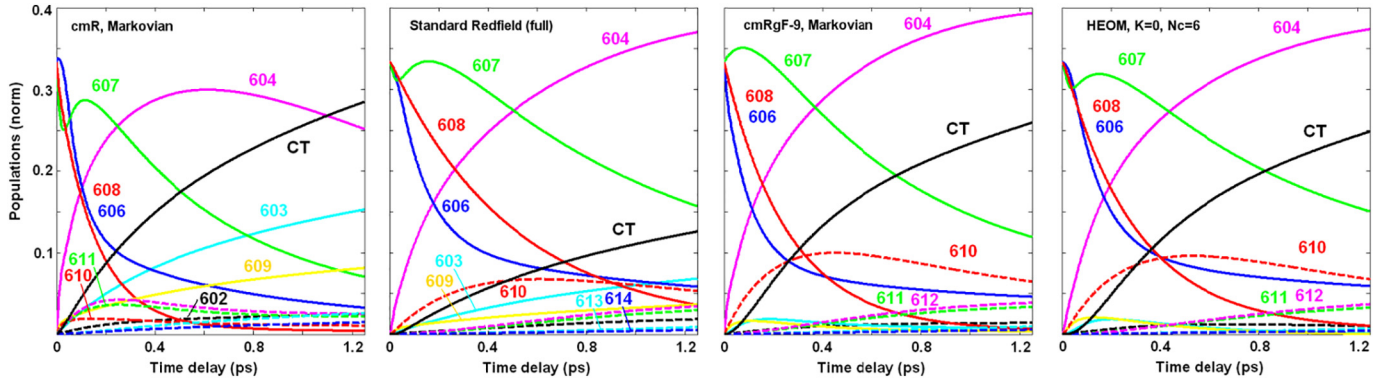

Fig. 6. Dynamics within the whole Lhca4 complex (N = 13 model) with initial *b*608 and coherent *b*606–607 excitation (with unperturbed site energies and V_{CT} = 3.2). Kinetics (on the timescale of 1.25 ps) are calculated with the cmR, sR, HEOM, and Redfield-Förster model cmRgF-9 (602–603, 604–606, 607, 608, 609, 610, 611–612, 613–614, CT).

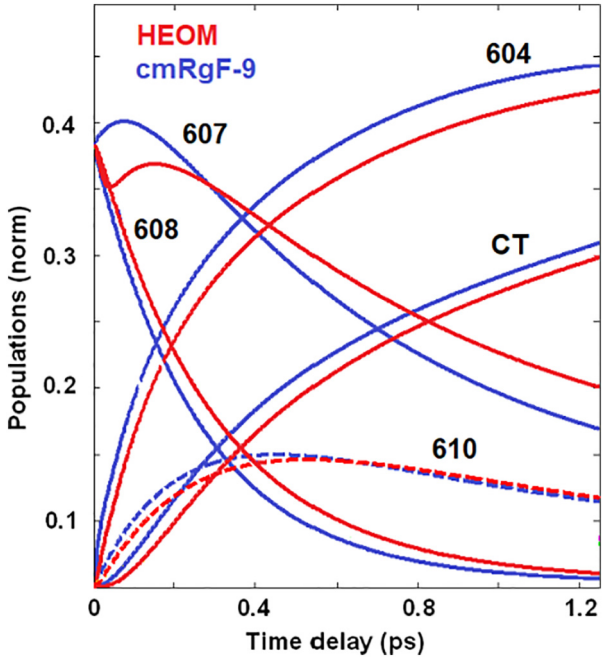

Fig. 7. The same as in Fig. 6, but with a quantitative comparison of the kinetics calculated with the HEOM (red lines) and the cmRgF-9 model (blue lines) in one frame.

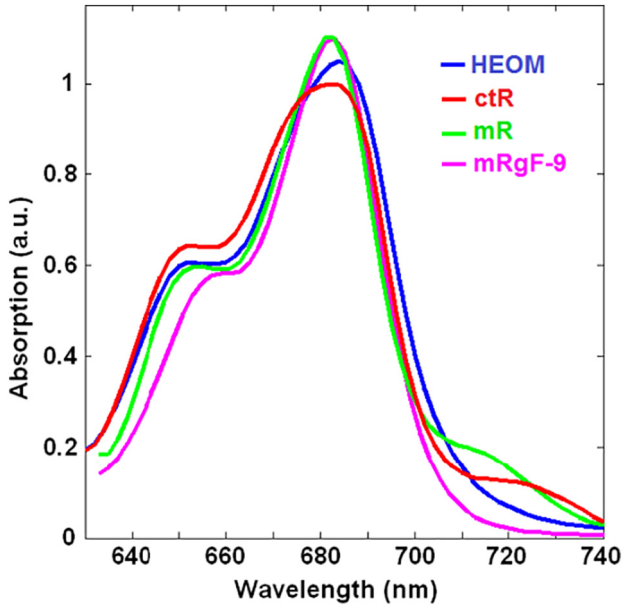

Fig. 8. Absorption spectra (for a single unperturbed realization of the disorder) calculated with HEOM, ctR, mR, and mRgF-9 (normalization of these spectra is slightly different). The mR and mRgF spectra are 3 nm red-shifted (to compensate for the dephasing shift not included into mR). The ratio of the phonon couplings for the CT and exciton states is 3.2. The exciton-CT coupling is 1.5 times increased (compared to Figs. 1–7) to make the red shoulder more discernible.

CT, but also containing significant dipole strength borrowed from the exciton states. In HEOM the red shoulder is not so intense because the excited states are now mixed with the displaced CT state, producing a dynamically localized lowest state with less borrowing of dipole strength (compare the mR/ctR and HEOM profiles in the 700–740 nm region in Fig. 8).

In the mRgF approach the spectrum is given by the sum of the spectra calculated with the mR theory for all the compartments. It means that we break some exciton couplings (in order to obtain more realistic kinetics) that can influence the spectral lineshapes. First, the red shoulder is absent at all (see mRgF-9 profile in Fig. 8), because there is no mixing with CT (so that the CT does not borrow dipole strength from the excited states) Second, after breaking of the exciton couplings some exciton states become less delocalized, and, correspondingly, their reorganization shift increases (for instance, the Chl *b* states are more red-shifted).

4. Discussion

4.1. Time scales of the CT population

The picture of energy transfers emerging from our modeling predicts fast population of the CT state after selective excitation of the sites strongly coupled to the CT. Thus, excitation of *a*603 results in CT population with a time constant of about 0.1 ps (for unperturbed site energies). Excitation of *a*609 (with subsequent *a*603–*a*609 equilibration within 50 fs) gives a similar time constant (about 0.15 ps) for the CT population (Fig. 3). Selective excitation of *a*602 (not so strongly coupled to *a*603 and *a*609) results in slower kinetics with a time constant of about 1 ps (data not shown).

Equilibration within the whole stromal-side compartment gives sub-ps transfers to the CT (determined by $b \rightarrow a$ transfers) and slower components (of a few ps) due to equilibration between the *a*610-*a*611-*a*612 and *a*602-*a*603-*a*609 clusters. Dynamics within the whole Lhca4 complex contains even slower components of the CT population determined by the slow transfers between the stromal- and lumenal-side layers with time constants of 10 ps or more, similarly to LHCII [34]. Kinetics of the CT population (corresponding to equilibration within the whole complex) are dominated by slow ps components. Notice that slow (5 ps) kinetics involving red spectral forms have been observed in Lhca4 experimentally [37,38].

4.2. Exciton-CT mixing and spectral lineshapes

Analysis of the spectra [22] revealed strong mixing of the excited and CT states in Lhca4. On the other hand, the CT state is dynamically localized as we demonstrate in this present study. Moreover, the states strongly coupled to CT become dynamically localized as well. Notice that these features are connected with anomalously big displacement of CT along nuclear coordinates, and do not depend on its energy. Thus we believe that not only red-shifted CTs, but also blue-shifted (with respect to the exciton states) CTs should be treated as dynamically localized. This greatly complicates the physical modeling of the antenna complexes. The energy transfer dynamics can be adequately described by breaking the exciton-type mixing between the localized states. The simplest (and numerically inexpensive) way to do it is using the combined Redfield-Förster approach. The Förster theory gives quite realistic rates of transfer between the dynamically localized states, but neglecting the mixing of the states results in the wrong exciton structure where some features are missed (for example, the red shoulder in the OD spectrum of Lhca4). Including all the excitonic interactions (as in the pure Redfield picture) gives the correct exciton structure, but fails to explain the kinetics.

In principle, the steady-state spectra of the complex can be described by mR (or ctR) theory, with simultaneous modeling of the kinetics using the cmRgF approach. This way one can expect a realistic picture for both the lineshapes and the kinetics. However, such an approach is not entirely consistent, because the exciton wavefunctions in cmRgF model are different from those of the mR/ctR model, thus leading to different dipole strengths and energies of the exciton components. The consistent description of the exciton spectra and the relaxation/reorganization dynamics requires more complicated approaches like HEOM. Compared to the mR picture, the HEOM gives not so intense mixing of the dynamically localized states (see red shoulder

in OD spectra shown in Fig. 8). It means that switching from the mR to HEOM the picture will require some adjustment of the parameters of the exciton-CT mixing (phonon couplings and disorder values for the CT, transition energy and the coupling of the CT to the excited states).

Notice in this respect that the Redfield picture suggests a scaling factor of 3.2 for the phonon coupling of the CT [22]. In principle one can expect that due to the big static dipole of the CT the scaling factor can be larger than 3 (i.e. up to 10 or even more). But within the Redfield model such a larger scaling factor (> 3–4) will result in too broad lineshapes. This is caused by an overestimation of the exciton-CT mixing (treated as uniform in the Redfield picture), giving too much borrowing of the phonon coupling from the CT. In the HEOM, where the mixing is described in a more realistic fashion, larger scaling factors result in reasonable linewidths (in contrast to the Redfield model). But the huge borrowing of the dipole strength by CT (as observed experimentally) is more difficult to explain in the HEOM picture, because the increase in reorganization energy (for a large scaling factor) breaks the exciton-CT mixing. Most likely, the value of the scaling factor emerging from a consistent HEOM picture will be larger than in the Redfield model (but probably not too large).

Another intriguing feature in the Lhca4 modeling is connected with the explanation of the red tail of the linear dichroism (LD) spectrum, which is difficult to do within the limits of the modified Redfield picture [22]. So far, there was no attempt to solve the problem with HEOM, but one may expect that this approach will give a deeper insight into the origin of the red tail of LD spectrum.

4.3. Compartmentalization schemes in Lhca4 and LHCII

The compartmentalization scheme developed in this work for Lhca4 is very similar to that of LHCII [27]. However, there is some difference due to presence of the CT state in Lhca4. In particular, in Lhca4 we have to break the coherent mixing between *a*603, *a*609, and CT. As a result, we need nine compartments (cmRgF-9 model), three more than for LHCII. Remarkably, the cmRgF-9 model gives quite reasonable dynamics, not much different from HEOM. This result indicates that the cmRgF-9 model can be used for calculating the nonlinear spectral responses for Lhca4 with a realistic spectral density and at arbitrary temperatures (which is difficult to do with HEOM, especially when evaluating the one to two-exciton absorption components of pump-probe and 2D-echo).

4.4. Nuclear coordinates and correlation of nuclear modes

In the schemes illustrating the configuration of the potential surfaces and their mixing (Figs. 2 and 3) we consider a simplified one-dimensional representation. This is useful in order to visualize the dynamics. But no assumption like that is made when modeling the real kinetics, i.e. we do not restrict to coupling of the electronic states to just one nuclear coordinate (when nuclear motions coupled with different states are correlated). In this section we wish to discuss how the nuclear degrees of freedom are accounted for and how the intersite correlations of the bath fluctuations are treated in different approaches used in our modeling.

In the standard Redfield theory the fluctuations induced by system-bath coupling can have an arbitrary radius of correlation [39,40], as well as in the modified Redfield [23,36] and complex time-dependent Redfield approaches [35]. Most popular is the model where the bath-induced fluctuations acting on different sites are uncorrelated [22,23,28,29,34,40–43]. Introducing a finite radius of correlation [36] is possible, as well as direct calculation of the correlations in site energy fluctuations for every pair of pigments [44]. Such a calculation for the FMO complex showed that the effect of these correlations on the exciton population dynamics and dephasing of coherences is negligible [44]. In all these versions of the Redfield theory the nuclear coordinates of the bath modes are not included as system coordinates, i.e. motion along these coordinates is not considered explicitly. The influence of the bath degrees of freedom is described as modulation of the site energies. This modulation is treated as a perturbation that induces a relaxation between the electronic (exciton) eigenstates. The perturbative character of the theory implies that the bath modes responsible for the exciton relaxation have no influence on the intrinsic properties of the exciton states (such as delocalization). In particular, the Redfield theory (in a pure exciton basis) is not capable to describe dynamic localization (i.e. localization induced by phonon reorganization), because the mixing of the electronic states is not dependent on the state of a phonon bath. This can be visualized as a mixing of the two potential surfaces equally displaced along any effective nuclear coordinate. This effective coordinate does not correspond to any of the real coordinates (that are not included explicitly at all). This is just a rough illustration needed to highlight a uniform (i.e. not dependent on nuclear coordinates) character of the mixing of the states.

The version of HEOM used in our modeling is derived supposing that nuclear modes acting on different sites are uncorrelated, i.e. each site has its own bath [30,31,45]. The manifold of the bath modes (described by an overdamped Brownian oscillator model) modulates the electronic energy of each site, as in Redfield theory. But in contrast to the Redfield approach the bath-induced fluctuations are taken into account nonperturbatively. Thus, the mixing of the electronic excitations is calculated with including the changes of the site energies induced by reorganization dynamics of all nuclear modes. This means that modulation of the site energy of any site changes the character of its mixing with other sites. In this way, the mixing of the sites depends on the state of their baths. In the HEOM the state of the bath is described by some number reflecting a combined action of a continuum of modes without considering explicitly their coordinates [30,45]. Such a model allows a description of dynamic localization if the two states have different couplings to phonons. Indeed, a larger reorganization shift of one site will break its mixing with another site and will localize the excitation near the bottom of its potential. But if the sites have equal phonon couplings, they will exhibit equal reorganization shifts, and therefore, the reorganization dynamics will not lead to dynamic localization (that is expected in the case of weakly coupled identical sites!). The situation resembles the mixing of the two potentials in the one-dimensional case: non-equal phonon couplings will cause different displacements of the potentials along some effective coordinate, thus allowing localization near their bottoms, whereas equal couplings corresponding to equal displacements will produce uniform mixing of the states (where the delocalization degree is not dependent on the nuclear coordinate). Notice again that this one-dimensional picture is useful only for illustrative purposes (there is no any effective coordinate used in the HEOM or Redfield model!)

The above-mentioned shortcoming with the description of dynamic localization is connected with the lack of explicit treatment of nuclear coordinates (which is impossible to do with a continuum of modes in the overdamped Brownian oscillator model). Restricting to a finite number of modes it is possible to build a more realistic picture, where the nuclear coordinates are included directly. In the case of N = 2 sites each nuclear mode is characterized by two coordinates, **x** and **y**, reflecting its coupling to the sites 1 and 2. Even for equal phonon couplings (when the potentials for the sites 1 and 2 are equally displaced along **x** and **y**, respectively) there may be dynamic localization induced by nuclear motion along the 'anticorrelated' direction $\mathbf{x} - \mathbf{y}$, connecting the bottoms of the potentials (these bottoms will not be mixed if the phonon reorganization energy exceeds the exciton coupling between the sites). The phenomenon can be described by the Redfield model in a multidimensional exciton-vibrational basis [46,47] or by HEOM with the spectral density containing underdamped vibrations [48].

Finally we note that the Förster theory implies uncorrelated phonons acting on localized sites [28,40,49]. In our modeling we use the combined Redfield-Förster theory where the bath-induced fluctuations

on different sites are supposed to be uncorrelated [29]. This is convenient for a comparison with the HEOM, where the bath modes acting on different sites are uncorrelated as well [30,45].

4.5. The role of the CT in light-harvesting

The question about the role of CT states in antenna complexes is still rather puzzling (for a review see [50]). The CT states can be used for quenching of extra excitations under high illumination. But in a non-quenching conformation (i.e. in normal antenna) the low lying CT acts like a trap. Notice however, that such traps can be useful keeping the excitation in the locations close to the final trap, i.e. the reaction center. Thus, in Lhca4 the CT localizes the excitation at the sites that are close to the linker Chls connecting the peripheral LHCI antenna with the PSI core [22]. In this way, the exciton-CT mixing is used to control the spectral properties of the antenna in order to optimize light-harvesting by creating directed energy transfers. The effectiveness of transfer between the exciton and CT states (including both trapping and detrapping from CT) is given by the degree of their mixing. The latter is determined an overlap of the phonon/vibrational wavefuncitons, that can be significantly increased if the vibrational energy is in resonance with the exciton-CT energy gap [47].

5. Conclusions

We develop the compartmentalization scheme for the Lhca4 antenna allowing a numerically inexpensive modeling of the energy transfer dynamics in the complex including equilibration between the bulk exciton levels and the red spectral forms (containing the CT states mixed with the excited-state manifold). We demonstrate that the combined Redfield-Förster approach gives a quantitatively correct description of the dynamics (including exciton-type relaxation within strongly coupled compartments and hopping-type migration between them) yielding the kinetics that are close to the exact HEOM solution. Comparison of the Redfield-Förster and HEOM methods shows that the CT state should be treated as dynamically localized. Besides, all the states within the strongly coupled cluster containing CT (i.e. the states mixed with each other and with CT) should be considered as dynamically localized as well. The proposed compartmentalization allows a calculation of various linear and nonlinear spectral responses with arbitrary spectral density using the Redfield-Förster approach.

Transparency document

The Transparency document associated with this article can be found, in online version.

Acknowledgements

V.N. was supported by the Russian Foundation for Basic Research (Grant No. 18-04-00105). R.C. was supported by the Foundation for Fundamental Research on Matter (FOM) and by the European Research Council via the ERC consolidator grant ASAP (281341). R. v. G. was supported by the VU University Amsterdam, the Laserlab-Europe Consortium, the TOP grant (700.58.305) from the Foundation of Chemical Sciences part of NWO, the advanced investigator grant (267333, PHOTPROT) from the European Research Council, and by the EU FP7 project PAPETS (GA 323901), and by his Academy Professor grant from the Netherlands Royal Academy of Sciences (KNAW).

References

[1] R. Croce, H. van Amerongen, Light-harvesting in photosystem I, Photosynth. Res. 116 (2013) 153–166.
[2] N. Nelson, W. Junge, Structure and energy transfer in photosystems of oxygenic photosynthesis, Annu. Rev. Biochem. 84 (2015) 659–683.
[3] P.E. Jensen, R. Bassi, E.J. Boekema, J.P. Dekker, S. Jansson, D. Leister, C. Robinson, H.V. Scheller, Structure, function and regulation of plant photosystem I, BBA-Bioenergetics 1767 (2007) (2007) 335–352.
[4] A. Ben-Shem, F. Frolow, N. Nelson, Crystal structure of plant photosystem I, Nature 426 (2003) (2003) 630–635.
[5] X. Qin, M. Suga, T. Kuang, J.-R. Shen, Structural basis for energy transfer pathways in the plant PSI-LHCI supercomplex, Science 348 (2015) 989–995.
[6] Y. Mazor, A. Borovikova, I. Caspi, N. Nelson, Structure of the plant photosystem I supercomplex at 2.6 Å resolution, Nat. Plants 3 (3) (2017) 17014.
[7] C. Slavov, M. Ballottari, T. Morosinotto, R. Bassi, A.R. Holzwarth, Trap-limited charge separation kinetics in higher plant photosystem I complexes, Biophys. J. 94 (2008) 3601–3612.
[8] E. Wientjes, I.H.M. van Stokkum, H. van Amerongen, R. Croce, The role of the individual Lhcas in photosystem I excitation energy trapping, Biophys. J. 101 (2011) 745–754.
[9] E. Molotokaite, W. Remelli, A.P. Casazza, G. Zucchelli, D. Polli, G. Cerullo, S. Santabarbara, Trapping dynamics in photosystem I-light harvesting complex I of higher plants is governed by the competition between excited state diffusion from low energy states and photochemical charge separation, J. Phys. Chem. B 121 (2017) 9816–9830.
[10] P. Akhtar, C. Zhang, Z.T. Liu, H.S. Tan, P.H. Lambrev, Excitation transfer and trapping kinetics in plant photosystem I probed by two-dimensional electronic spectroscopy, Photosynth. Res. 135 (2018) 239–250.
[11] V.H.R. Schmid, K.V. Cammarata, B.U. Bruns, G.W. Schmidt, In vitro reconstitution of the photosystem I light-harvesting complex LHCI-730: heterodimerization is required for antenna pigment organization, Proc. Natl. Acad. Sci. U. S. A. 94 (1997) 7667–7672.
[12] H. Zhang, H.M. Goodman, S. Jansson, Antisense inhibition of the photosystem I antenna protein Lhca4 in Arabidopsis thaliana, Plant Physiol. 15 (1997) 1525–1531.
[13] U. Ganeteg, A. Strand, P. Gustafsson, S. Jansson, The properties of the chlorophyll *a*/*b*-binding proteins Lhca2 and Lhca3 studied in vivo using antisense inhibition, Plant Physiol. 127 (2001) 150–158.
[14] S. Castelletti, T. Morosinotto, B. Robert, S. Caffarri, R. Bassi, R. Croce, Recombinant Lhca2 and Lhca3 subunits of the photosystem I antenna system, Biochemistry 42 (2003) 4226–4234.
[15] E. Wientjes, R. Croce, The light-harvesting complexes of higher-plant photosystem I: Lhca1/4 and Lhca2/3 form two red-emitting heterodimers, Biochem. J. 433 (2011) 477–485.
[16] J.A. Ihalainen, M. Ratsep, P.E. Jensen, H.V. Scheller, R. Croce, R. Bassi, J.E.I. Korppi-Tommola, A. Freiberg, Red spectral forms of chlorophylls in green plant PSI: a site-selective and high pressure spectroscopy study, J. Phys. Chem. B 107 (2003) 9086–9093.
[17] T. Morosinotto, J. Breton, R. Bassi, R. Croce, The nature of a chlorophyll ligand in Lhca proteins determines the far red fluorescence emission typical of photosystem I, J. Biol. Chem. 278 (2003) 49223–49229.
[18] T. Morosinotto, M. Mozzo, R. Bassi, R. Croce, Pigment–pigment interactions in Lhca4 antenna complex of higher plants photosystem I, J. Biol. Chem. 280 (2005) 20612–20619.
[19] R. Croce, A. Chojnicka, T. Morosinotto, J.A. Ihalainen, F. van Mourik, J.P. Dekker, R. Bassi, R. van Grondelle, The low-energy forms of photosystem I light-harvesting complexes: spectroscopic properties and pigment–pigment interaction characteristics, Biophys. J. 93 (2007) 2418–2428.
[20] E. Romero, M. Mozzo, I.H.M. van Stokkum, J.P. Dekker, R. van Grondelle, R. Croce, The origin of the low-energy form of photosystem I light-harvesting complex Lhca4: mixing of the lowest exciton with a charge-transfer state, Biophys. J. 96 (2009) L35–L37.
[21] Z. Liu, H. Yan, K. Wang, T. Kuang, J. Zhang, L. Gui, X. An, W. Chang, Crystal structure of spinach major light-harvesting complex at 2.72 A resolution, Nature 428 (2004) 287–292.
[22] V.I. Novoderezhkin, R. Croce, Md. Wahadoszamen, I. Polukhina, E. Romero, R. van Grondelle, Mixing of exciton and charge-transfer states in light-harvesting complex Lhca4, Phys. Chem. Chem. Phys. 18 (2016) 19368–19377.
[23] W.M. Zhang, T. Meier, V. Chernyak, S. Mukamel, Exciton-migration and three-pulse femtosecond optical spectroscopies of photosynthetic antenna complexes, J. Chem. Phys. 108 (1998) 7763–7774.
[24] Q. Ai, Y.-J. Fan, B.-Y. Jin, Y.-C. Cheng, An efficient quantum jump method for coherent energy transfer dynamics in photosynthetic systems under the influence of laser fields, New J. Phys. 16 (2014) 053033.
[25] Y.-H. Hwang-Fu, W. Chen, Y.-C. Cheng, A coherent modified Redfield theory for excitation energy transfer in molecular aggregates, Chem. Phys. 447 (2015) 46–53.
[26] Y. Chang, Y.-C. Cheng, On the accuracy of coherent modified Redfield theory in simulating excitation energy transfer dynamics, J. Chem. Phys. 142 (2015) 034109.
[27] V.I. Novoderezhkin, R. van Grondelle, Modeling of excitation dynamics in photosynthetic light-harvesting complexes: exact vs perturbative approaches, J. Phys. B Atomic Mol. Phys. 50 (2017) 124003.
[28] V.I. Novoderezhkin, R. van Grondelle, Spectra and dynamics in the B800 antenna: comparing hierarchical equations, Redfield and Förster theories, J. Phys. Chem. B 117 (2013) 11076–11090.
[29] V.I. Novoderezhkin, R. van Grondelle, Physical origins and models of energy transfer in photosynthetic light harvesting, Phys. Chem. Chem. Phys. 12 (2010) 7352–7365.
[30] A. Ishizaki, Y. Tanimura, Quantum dynamics of system strongly coupled to low-temperature colored noise bath: reduced hierarchy equations approach, J. Phys. Soc. Jpn. 74 (2005) (2005) 3131–3134.
[31] J. Zhu, S. Kais, P. Rebentrost, A. Aspuru-Guzik, Modified scaled hierarchical

equation of motion approach for the study of quantum coherence in photosynthetic complexes, J. Phys. Chem. B 115 (2011) 1531–1537.
[32] C. Kreisbeck, T. Kramer, A. Aspuru-Guzik, Scalable high-performance algorithm for the simulation of exciton dynamics. Application to the light-harvesting complex II in the presence of resonant vibrational modes, J. Chem. Theory Comput. 10 (2014) 4045–4054.
[34] V.I. Novoderezhkin, A. Marin, R. van Grondelle, Intra- and inter-monomeric transfers in the light harvesting LHCII complex: the Redfield-Förster picture, Phys. Chem. Chem. Phys. 13 (2011) 17093–17103.
[35] A. Gelzinis, L. Valkunas, F.D. Fuller, J.P. Ogilvie, S. Mukamel, D. Abramavicius, New J. Phys. 15 (2013) 075013.
[36] G. Raszewski, W. Saenger, T. Renger, Theory of optical spectra of photosystem II reaction centers: location of the triplet state and the identity of the primary electron donor, Biophys. J. 88 (2005) 986–998.
[37] A.N. Melkozernov, S. Lin, V.H.R. Schmid, H. Paulsen, G.W. Schmidt, R.E. Blankenship, Ultrafast excitation dynamics of low energy pigments in reconstituted peripheral light-harvesting complexes of photosystem I, FEBS Lett. 471 (2000) 89–92.
[38] J.A. Ihalainen, R. Croce, T. Morosinotto, I.H.M. van Stokkum, R. Bassi, J.P. Dekker, R. van Grondelle, Excitation decay pathways of Lhca proteins: a time-resolved fluorescence study, J. Phys. Chem. B 109 (2005) 21150–21158.
[39] T. Renger, V. May, O. Kühn, Ultrafast excitation energy transfer dynamics in photosynthetic pigment-protein complexes, Phys. Rep. 343 (2001) 137–254.
[40] M. Yang, G.R. Fleming, Influence of phonons on exciton transfer dynamics: comparison of the Redfield, Förster, and modified Redfield equations, Chem. Phys. 275 (2002) 355–372.
[41] V.I. Novoderezhkin, M.A. Palacios, H. van Amerongen, R. van Grondelle, Energy-transfer dynamics in the LHCII complex of higher plants: modified Redfield approach, J. Phys. Chem. B 108 (2004) 10363–10375.
[42] O. Kühn, V. Sundström, Pump–probe spectroscopy of dissipative energy transfer dynamics in photosynthetic antenna complexes: a density matrix approach, J. Chem. Phys. 107 (1997) 4154–4164.
[43] O. Kühn, V. Sundström, T. Pullerits, Fluorescence depolarization dynamics in the B850 complex of purple bacteria, Chem. Phys. 275 (2002) 15–30.
[44] T. Renger, A. Klinger, F. Steinecker, M. Schmidt Am Busch, J. Numata, F. Müh, Normal mode analysis of the spectral density of the Fenna – Matthews – Olson light-harvesting protein: how the protein dissipates the excess energy of excitons, J. Phys. Chem. B 116 (2012) 14565–14580.
[45] A. Ishizaki, G.R. Fleming, Unified treatment of quantum coherent and incoherent hopping dynamics in electronic energy transfer: reduced hierarchy equation approach, J. Chem. Phys. 130 (2009) 234111.
[46] M. Ferretti, V.I. Novoderezhkin, E. Romero, R. Augulis, A. Pandit, D. Zigmantas, R. van Grondelle, The nature of coherences in the B820 bacteriochlorophyll dimer revealed by two-dimensional electronic spectroscopy, Phys. Chem. Chem. Phys. 16 (2014) 9930–9939.
[47] V.I. Novoderezhkin, E. Romero, J. Prior, R. van Grondelle, Exciton-vibrational resonance and dynamics of charge separation in the photosystem II reaction center, Phys. Chem. Chem. Phys. 19 (2017) 5195–5208.
[48] M. Tanaka, Y. Tanimura, Quantum dissipative dynamics of electron transfer reaction system: nonperturbative hierarchy equations approach, J. Phys. Soc. Jpn. 78 (2009) 073802.
[49] T. Förster, Delocalized excitation and excitation transfer, in: O. Sinanoğlu (Ed.), Modern Quantum Chemistry, Part III. B. Light and Organic Crystals, Academic Press, New York, 1965, pp. 93–137.
[50] J.R. Reimers, et al., Challenges facing an understanding of the nature of low-energy excited states in photosynthesis, BBA-Bioenergetics 1857 (2016) 1627–1640.